DTU Library

Dependence of the Al Distribution in CHA Zeolite on the Presence of Na$^+$ during the Synthesis.
An EPR Investigation of Cu Species in CuCHA

Gao, Qi; Nielsen, David; Mossin, Susanne

[Link back to DTU Orbit](#)

ChemCatChem

Research Article
doi.org/10.1002/cctc.202301377

Chemistry
Europe
European Chemical
Societies Publishing

www.chemcatchem.org

Dependence of the Al Distribution in CHA Zeolite on the Presence of Na$^+$ during the Synthesis. An EPR Investigation of Cu Species in CuCHA

Qi Gao,[a] David Nielsen,[a] and Susanne Mossin*[a]

Copper-exchanged zeolites, such as CuCHA are active catalysts for removing NO and NO$_2$ from automotive exhaust. The zeolite synthesis is decisive for the aluminium distribution in the framework and the properties of the catalyst. We have applied in-situ EPR spectroscopy on CuCHA based on CHA synthesized in four different ways. We found that different mineralizing agents led to differences in the Cu distribution in the final product. Several distinct Cu sites were present after thermal activation according to the EPR spectra and we found that the presence of Na$^+$ during the synthesis boosted the forming of "paired" Al close to Cu, but at the same time limited the ion-exchange capacity and the redox activity. Two types of well-defined EPR spectra were found, Site A and Site B. Site B was redox active and catalytically active for all investigated materials whereas the properties of Site A depended on the CHA material and consisted of two subtypes distinguished by their reactivity towards NO and NH$_3$. Studies with isotope labeled NH$_3$ showed that the system was highly dynamic. In-situ EPR was proved to be an excellent spectroscopic technique to investigate the Cu distribution directly and investigate the Al distribution indirectly for CuCHA zeolites.

Introduction

Cu-exchanged zeolites such as Cu-SSZ-13 with chabazite morphology are employed in diesel exhaust gas cleaning. The industrial interest is driven by strict regulations on the emission of NO$_x$ due to its role in smog formation and its negative effects on human health and the environment.[1,2]

Cu-zeolites are active catalysts in the selective catalytic reduction of NO$_x$ by NH$_3$.[3] An aqueous solution of urea is used as an NH$_3$ source and is sprayed into the hot exhaust from the combustion chamber where it decomposes to NH$_3$ and CO$_2$. The use of CuCHA as the active catalyst has replaced the prior state-of-the-art catalysts in automotive applications due to the larger range of temperatures where the CuCHA is active and due to the higher hydrothermal stability than other zeolite catalysts.

CuCHA materials have been studied thoroughly. Investigations described in the literature have used EPR, H$_2$-TPR, X-ray absorption spectroscopy, and IR spectroscopy as well as other methods.[4–8] Despite this, the active Cu sites and the catalytic mechanism have not yet been fully understood.[6–10] One reason that may contribute to the lack of clarity is the dynamic nature

of the active sites[9,11] and the different properties of the zeolite materials investigated. The conditions under which the catalyst is measured, and the pre-treatments of the catalysts significantly influence the obtained results.[4–8] A reason for the elusive nature of the copper exchanged zeolites is the dependence of the ion exchange properties on the different synthesis conditions used for preparing the zeolite material, particularly the presence of sodium ions during crystallization. The concentration of sodium ions affects the Al distribution and thus, the distribution of copper in the final product.[12] In this work, we investigate how the varying synthesis methods reported in literature affect the Al-distribution and final Cu-speciation in the catalyst systems as mapped by in-situ Electron Paramagnetic Resonance (EPR) of the paramagnetic Cu^{2+} centers. The EPR response is sensitive to the exact coordination environment of copper and also provides the ability to quantify the amount of the individual copper sites present. In this work we review the literature results and compare the reported EPR spectra to measured EPR spectra of CuCHA materials based on CHA zeolites synthesized by three different methods differing in the mineralizing agent: The OH-route, the HF-route, and the NaOH-route as well as a commercial CHA zeolite product. The results contribute to a further understanding of the CuCHA SCR catalyst system.

Synthesis methods

The synthesis of SSZ-13, a CHA zeolite with variable Si/Al ratio was originally patented by Zones in 1985.[13] The synthesis method was since then adapted and varied by several groups. The general method is to mix Si- and Al-sources in an aqueous solution of NaOH and a structure-directing agent (SDA). The

[a] Q. Gao, D. Nielsen, S. Mossin
Centre for Catalysis and Sustainable Chemistry, Department of Chemistry, Technical University of Denmark, Kemitorvet 207, 2800 Kgs. Lyngby, Denmark
E-mail: slmo@kemi.dtu.dk

ChemCatChem

Research Article
doi.org/10.1002/cctc.202301377

Chemistry
Europe

European Chemical
Societies Publishing

slurry is heated to form a gel which is transferred to an autoclave and heated for several days to crystalize the zeolite framework around the SDA. The resulting zeolite is washed and calcined to burn away the SDA. Variations in the general process include the use of different mineralizing agents and variation of the Na$^+$: SDA ratio. It is also possible to use another mineralizing agent or to omit Na$^+$ in the synthesis gel.[12,14]

The CHA topology is comprised of double six-membered rings (d6r) of silicon and aluminum tetrahedral sites (T-sites) with corner-sharing oxygen atoms, see Figure 1. The d6r are stacked in an A-B-C pattern and between the d6r, large cages are formed by connections of the d6r by eight-membered rings of T-sites.[16] When an Al^{3+} replaces a Si^{4+} an extra negative charge is formed. The negative charge associated with Al in the framework can be balanced by extra framework cations such as H$^+$, Na$^+$, Cu$^+$, or Cu^{2+}. A Cu^{2+} ion requires two Al sites or one Al and one extra-framework OH$^-$ for charge balance. If two Al atoms are placed in the same six-membered ring (6mr), then according to Lövensteins rule,[18] these Al atoms must be located with a minimum of one Si atom in between them due to the charge density being too high for two Al^{3+} only separated by O. Thus, the two Al atoms in a 6mr can be placed directly across from each other in a "para" position or with one Si between them in a "meta" position. They are referred to

jointly as Z$_2$Cu. If Cu^{2+} is charge-balanced by OH$^-$ in addition to a single framework Al, the site is referred to as ZCuOH.

We have chosen here to focus on the following three synthetic protocols that are representative of many of the investigated materials in the literature. For the selected materials, detailed EPR data are presented by us or are available in the literature. An overview of the synthetic protocols are given in Table 1.

NaOH-route

The synthesis of CHA materials by the NaOH-route is the synthesis as originally patented by Zones et al.[13] The typical SDA is N,N,N-trimethyl-1-adamantylammonium (TMAda$^+$) with hydroxide as the counter ion in an aqueous solution. The method may be applied with a varying NaOH concentration and variations of silicon and aluminum precursors. The NaOH-route can be applied to synthesize materials with Si/Al ratios of 10–65.[12] Lower Si/Al ratios tend to yield materials with more extra framework aluminum. Gounder et al.[14] report that the Na$^+$:SDA ratio has a direct influence on the final Al distribution such that a higher Na$^+$:SDA ratio results in more paired Al sites in the resulting SSZ-13 material. The groups of Gao, Peden, and Gounder are using materials produced by this method.[14,19–23]

OH-route, sodium-free

The OH-route has been reported by Gounder et al.[14] and is essentially a variation of the NaOH-route above where Na$^+$:SDA ratio is zero. Si/Al ratios of 15–30 have been achieved by the sodium-free OH-route. The resulting zeolite materials are reported to only contain ZCuOH sites according to Di Iorio and Gounder. This conclusion is based primarily on the Co^{2+} titration method.[14,22]

HF-route, sodium-free

In the HF-route, HF is added as the mineralizing agent.[24,25] For the synthesis with HF, no sodium is present and the resulting CHA materials have been reported to have Si/Al ratios in the range from 12 to >100. The CHA zeolites made in HF-media tend to have fewer defects than their OH-media counterparts and higher Si/Al ratios can be achieved.[25,26] The HF-route yields the H-form of the zeolite and therefore ion exchange with NH$_4^+$ and the subsequent calcination step can be avoided. On the downside, the HF-route requires the handling of HF, which is undesirable in an industrial setting. This material has been the target of many investigations by the Bordiga, Lamberti, Vennestrøm, and Beato groups as well as by our own group.[5,7,27–29]

Other methods include inter-zeolite transformation where FAU is converted to CHA with high Al content. Typically Si/Al is lower than 8.[12] It is also possible to exclude the ion-exchange step by synthesizing the CuCHA in a one-pot synthesis:[30,31]
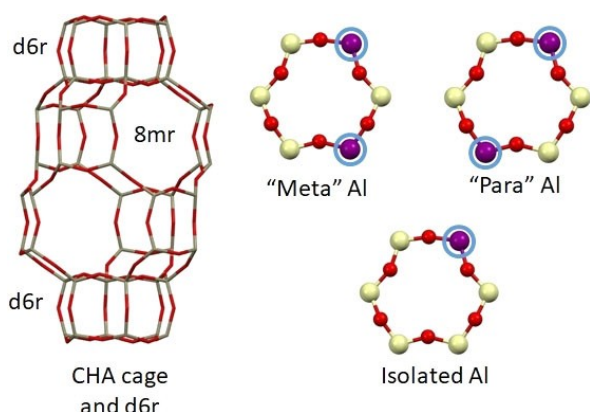
Figure 1. Illustration of the CHA framework. To the left a CHA-cage with double six-membered rings (d6r) on top and bottom. The eighth-membered rings (8mr) forming the channels are also visible. To the right are six-membered rings with Al atoms (purple) placed in various positions.[15–17] Color code: Red = O, white = Si, purple = Al.

Table 1. Overview of different precursors used in the synthesis methods.

	HF-route	OH-route	NaOH-route
Al-precursor	Al$_2$O$_3$ or Al(O-i-Pr)$_3$	Al(OH)$_3$	Al(OH)$_3$
Si-precursor	TEOS (= Si(OEt)$_4$)	Colloidal SiO$_2$	Colloidal SiO$_2$
SDA	TMAdaOH	TMAdaOH	TMAdaOH
Other ingredients	HF	–	NaOH
Reference	[24,25]	[14]	[14]

TEOS = tetraethyl orthosilicate, TMAda = N,N,N-trimethyl-1-adamantylammonium, O-i-Pr = isopropoxide.

Here, Cu is added directly to the synthesis gel as a Cu coordination compound, tetraethylenepentaamine copper(II). The one-pot method can be applied both in NaOH-media and in NH$_4$F media and the Si/Al ratio is controllable. So far, these materials have not been investigated using in-situ EPR and will not be mentioned further here.

The morphologies of the CHA materials are typically described as fine crystalline powders and the individual crystallites are pseudo-rhombohedral, almost cube-shaped in appearance[17] when investigated by TEM/SEM. Not all report the morphology of the materials, but the variations in morphology between the different synthetic methods do not appear to be significant.

EPR investigations of CuCHA

The CuCHA catalyst materials have received much attention and several groups have investigated CuCHA using EPR spectroscopy.[10,11,31–34] In general, it is observed that the EPR spectrum of a CuCHA catalyst changes when exposed to different conditions. Thus, one type of spectral feature is observed for a sample exposed to ambient conditions, where the zeolite spontaneously absorbs moisture and oxygen is available. The EPR spectrum changes dramatically when the catalyst is heated in a flow of air yielding new Cu species with corresponding sets of spectral features. After exposure to reactant gases, the EPR response will change again reflecting the change in the local coordination of the predominant copper species. In this way species, such as [Cu(NH$_3$)$_4$]$^{2+}$ and CuNO$_3$-species have been observed.[7,27] The interpretation of spectra is complicated by some Cu sites being EPR inactive and therefore not showing up in the observed spectra. If copper is reduced to diamagnetic Cu$^+$, clearly no spectrum is expected. In addition, Cu^{2+} with a strong antiferromagnetic coupling to another Cu^{2+} such as in a Cu–O–Cu dimer is expected to be EPR inactive. Specifically relevant for Cu in the vicinity of only one charge compensating Al site, three-coordinate Cu^{2+} with two zeolite contacts and one OH-group is expected to be EPR inactive due to the pseudo-Jahn-Teller effect which leads to a fast relaxation of the excited spin state.[34,35,35,36]

In this study, we focus on the EPR spectra of thermally activated CuCHA materials. The observed EPR spectra can be described using an axial spin Hamiltonian with $S=1/2$ corresponding to one unpaired electron and $I=3/2$ due to the interaction of the unpaired electron with the nuclear spin of both Cu isotopes, see Eq. 1.

$$H = g_{\parallel}\mu_B S_z B_Z + g_{\perp}\mu_B \left(S_x B_x + S_y B_y\right) + A_{\parallel}S_z I_z + A_{\perp}\left(S_x I_x + S_y I_y\right) \quad (1)$$

Here $g_{\parallel}$ and $g_{\perp}$ are the g-values along the parallel and perpendicular axes, μ_B is the Bohr magneton, S_i are the components of the electron spin operator, B_i are the magnetic field components in each axis direction, $A_{\parallel}$, and $A_{\perp}$ are the hyperfine coupling constants and I_i are the nuclear spin components, where $i=$x,y,z. The parallel features are well resolved in the EPR spectra whereas the perpendicular features overlap with each other and are more featureless. The set of parameters reported are $A_{\parallel}$ and $g_{\parallel}$ for each Cu species observed.

The parallel spin Hamiltonian values in CuCHA materials are slightly temperature dependent. This is likely due to thermal expansion of the framework distorting the Cu coordination geometry. It is observed that the g-values increase and the A-values decrease with increasing temperature. Furthermore, the distribution of different EPR active Cu-sites depend on the copper loading and Si/Al ratio of the material. Being aware of these effects on the spin Hamiltonian parameters and copper site distribution, the literature was searched for EPR spectra of CuCHA synthesized by different methods, see Table 2.

The observed Cu species listed in Table 2 are labeled either Site A or Site B. These has previously been assigned to Cu^{2+} in Z$_2$Cu sites in the d6r with 2Al in the "meta" and "para" position of one 6mr.[34,36] For low Si/Al and/or low Cu/Al only Site B is observed in the EPR spectra after thermal activation. This is the case for CuCHA with Si/Al$=6$ and Cu/Al$=0.03$ by Peden et al. using CHA synthesized by the inter-zeolite transformation method[10] and for CuCHA with Si/Al$=12$ and Cu/Al$=\sim0.35$ by Gao et al. with CHA synthesized with Na$^+$ present.[38] For these studies, the spin Hamiltonian parameters were not reported, but inspection of the published spectra reveal that mainly one

Table 2. Overview of spin Hamiltonian values observed on thermally activated CuCHA synthesized by different methods. N.O. = Not Observed. RT = Room Temperature.

Synthesis route	Site A		Site B		Temperature of measurement [°C]	Pretreatment: Gas/Temperature [°C]	Si/Al	Cu/Al	Reference
	$g_{\parallel}$	$A_{\parallel}$ [MHz]	$g_{\parallel}$	$A_{\parallel}$ [MHz]					
HF	2.325	487	2.358	464	RT	O$_2$ / 250	15	0.1–0.5	[27,34]
NaOH	N.O.	N.O.	2.368	427	250	O$_2$/300	16	0.1	[11]
NaOH	2.321	445	2.368	427	250	O$_2$/300	16	0.3	[11]
NaOH	N.O.	N.O.	2.36	438	50	N$_2$/250	6	0.1	[19]
NaOH	N.O.	N.O.	2.36	456	RT	N$_2$/300	6	0.1	[36]
NaOH	2.32	513	2.36	456	RT	N$_2$/300	36	0.2	[36]
One-pot (Na$_2$O)	N.O.	N.O.	2.35	493	−168	Vac./450	9	0.6	[37]

Cu-signal was observed in the EPR spectra after thermal activation.

Results

In the following, samples are denoted by CuCHA followed by letters indicating the zeolite synthesis methods and finally an indication of how Cu was added. The zeolite synthesis is indicated by Na for H-CHA from the NaOH-route, OH for the OH-route, HF for the HF-route and COM for the commercial material. The method of Cu addition is indicated with the concentration of the ion-exchange solution for the ion-exchanged samples and IMP for the impregnated sample. With this notation, CuCHA-Na-0.1 is the CuCHA material prepared from H-CHA from the NaOH-route and ion-exchanged with a 0.1 mM Cu^{2+} solution, CuCHA-OH-IMP is the CuCHA material prepared from H-CHA from the OH-route impregnated with Cu^{2+} solution to achieve 4.0 wt.% Cu.

X-ray powder diffraction was measured for synthesized and commercial samples. The obtained diffractograms confirm that the synthesis resulted in microcrystalline CHA materials, see Figure 2.

All characteristic peaks for CHA are observed on both the synthesized and the commercial samples. The relative intensities of the reflections deviate slightly between the samples due to the difference in particle sizes and morphology. The NaOH route sample has an extra peak marked with a red diamond in Figure 2.

The TEM images reveal differences in the morphology of the NaOH-route CHA, Figure 2B and the OH-route CHA, Figure 2C. The NaOH-route CHA is shaped as rhombohedral crystals, whereas the OH-route CHA is predominantly shaped like spherical particles made of smaller rhombohedral or cubic-like crystals. For the 50 mM Cu-exchanged OH-route CHA, neither Cu clusters nor nanoparticles of CuO are observed in the TEM image. The average particle size of the OH-route zeolite is $1.13\,\mu m \pm 0.17\,\mu m$. For the NaOH-route material, a portion of the crystals have one edge significantly shorter than the rest, forming slabs.

The powdered Cu-exchanged samples were analyzed by XRF, see Table S1. There is no residue Na in the NaOH-route CHA. The Si/Al ratios are determined by XRF to be Si/Al = 11.7(7) for the OH-route CHA and Si/Al = 5.8(1) for the NaOH-route CHA.

Solid-state NMR spectra are shown in Figures S1 and S2. The Si/Al ratios of the framework are estimated by solid-state ^{29}Si NMR and ^{27}Al NMR to be Si/Al = 13.2 for the OH-route sample and Si/Al = 8.4 for the NaOH-route samples. Both materials show a discrepancy between the NMR and XRF results, and the difference is more pronounced for the samples synthesized by the NaOH-route. The XRF analysis includes all Al in the sample, whereas the NMR analysis only took framework Al into account. The large main peak observed in the ^{27}Al NMR spectra for both samples at ~60 ppm corresponds to framework Al and the peak at around 1 ppm shows the presence of extra-framework Al. There is a significant amount of extra framework Al in the NaOH-route CHA. Estimated from the difference in the reported XRF and NMR results, the amount of extra framework Al in the CHA synthesized by the NaOH-route is approximately 30% of the total Al in the sample. For OH-route CHA, the amount of extra framework Al is around 11%. The NaOH-route CHA was synthesized several times to determine the reproducibility of the amount of extra-framework Al and we found approximately the same amount each time when using the literature synthetic method. It was decided to proceed with the sample despite this imperfection to include also the influence of extra-framework Al in the study of the EPR response.

Quantification by ICP and EPR

For selected samples synthesized by the OH-route and by the NaOH-route, the Cu content was determined by ICP-OES and by ex-situ EPR as described below, see Table 3.

For the ion-exchanged samples the values obtained from EPR and ICP differ by up to 30%. The EPR values are higher than the ICP values for all the ion-exchanged samples. Previous measurements show EPR quantification to be accurate but to
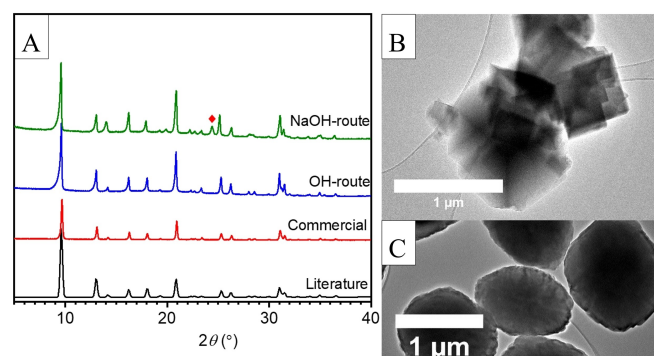

Figure 2. A: Powder XRD diffractograms of synthesized H-CHA from the NaOH-route (green), from the OH-route (blue); commercially available H-CHA (red) and reference diffractogram (black).[26] B: TEM image of the Na-CHA from NaOH synthesis, C: TEM-image of the OH-route CuCHA after ion exchange by 50 mM Cu^{2+} solution, wash, drying, and calcination.

Table 3. Cu content as determined by ICP and EPR. IMP are the samples that were impregnated to contain 4 wt.% Cu.

Cu^{2+} conc. during ion exchange		0.1 mM	0.5 mM	1.0 mM	5.0 mM	50 mM	500 mM	IMP.
OH-route CHA	Cu by ICP [wt.% Cu]		0.3		0.7	1.0	1.8	3.4
	Cu by EPR [wt.% Cu]		0.5		1.0	1.5	2.5	2.3
NaOH-route CHA	Cu by ICP [wt.% Cu]	0.1		0.5		1.0	1.5	3.9
	Cu by EPR [wt.% Cu]	0.1		0.8		1.4	1.7	1.9

systematically overestimate the Cu content by up to 0.25 wt.% Cu when using our method of integrating and comparing to a solid Cu reference material. A flat line with no EPR signal still has non-zero intensity after the double integration performed in the analysis because of random noise on the measured spectrum.[27,35] The values can be corrected using calibration curves based upon prior knowledge to obtain a more precise value of the copper content in the individual samples, see Figure S3. The ICP results presented here were obtained with a mild digestion of the sample without the addition of HF since the HF-digestion step is highly problematic from a safety point of view and is best avoided if possible. The values systematically underestimate the Cu content since a remnant of Cu was not extracted for analysis. The impregnated samples that are known to contain exactly 4.0 wt.% Cu according to the synthesis were found to contain 3.4 and 3.9 wt.% Cu according to ICP for the OH-route and NaOH-route CuCHA, respectively. EPR observes even less, 2.3 and 1.9 wt.% Cu, due to the formation of EPR inactive species. In conclusion, for the ion-exchanged samples, we believe the true values of the Cu content of ion-exchanged samples are found between the results from ICP and from EPR, see Figure S3. For the impregnated samples, we know the Cu content and both methods underestimate the content. In the following we will report the uncorrected values from the EPR investigation since the overestimation is systematic and all our conclusions are based on comparison between the EPR response of similar samples treated in the same way. The values obtained directly from the described analysis are sufficient for this purpose.

The EPR active Cu in fresh CuCHA samples prepared by ion-exchange exhibits an upper limit for both series. For CuCHA-Na-50 the value is 1.4 wt.% Cu and for CuCHA-Na-500 it is 1.7 wt.% Cu despite the 10x higher concentration of Cu^{2+} during ion-exchange. For CuCHA-OH-50 the value is 1.5 wt.% Cu and for CuCHA-OH-500 it is 2.5 wt.% Cu. The Cu wt.% (as determined by EPR) for the fresh samples is plotted vs. the copper concentration in the ion exchange solution in Figure 3.

In CuCHA-Na-IMP and CuCHA-OH-IMP the total amount of Cu exceeds the ion-exchange capability of the materials and not all are observable by EPR. For the NaOH-route materials, the IMP sample contains more EPR active Cu than the highest amount obtained by voluntary ion-exchange whereas for the OH-route samples, the opposite is observed. Cu is clearly more readily exchanged into the OH-route CHA than into the NaOH-route CHA. This difference is not due to Na^+ ions in the NaOH-route material "blocking" the diffusion pathway for $Cu^{2+}(aq)$ during ion-exchange, since, by XRF analysis, there is no sodium present in either of the H-form parent zeolites. Rather, an explanation must be sought in the compatibility of the charge distribution in the H-form zeolite with $Cu^{2+}(aq)$ and therefore with the Al distribution in the zeolite and the control of pH during the ion-exchange process. We also conclude that the EPR active Cu after simple impregnation is not distributed well in the zeolite. Approximately half of the Cu is caught in some type of EPR inactive sites even after calcination and subsequent equilibration at ambient conditions with oxygen and moisture present.
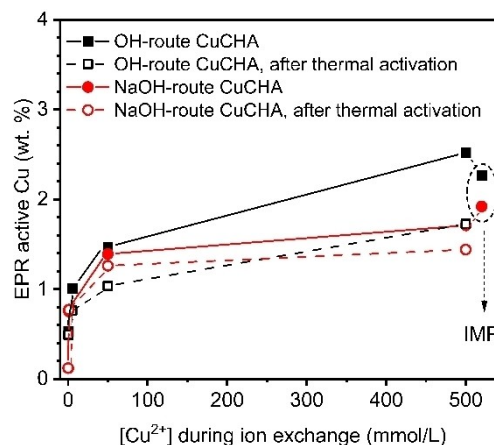

Figure 3. EPR active Cu for the fresh samples and the in-situ thermally activated samples plotted versus the $[Cu^{2+}]$ concentration during ion exchange. The black squares correspond to CHA from the OH-route synthesis and the red circles correspond to the CHA from the NaOH-route synthesis. The fresh samples prepared by impregnation (with 4 wt.% Cu) are marked IMP.

After the thermal activation, the intensity of the EPR spectrum decreases for all samples. The reduction of Cu^{2+} to Cu^+ is an unlikely reason for the loss of the EPR signal since 10% O_2 is present during the thermal activation and other methods such as X-ray absorption indicate no reduction of Cu^{2+} to Cu^+ with this treatment. Thus, the loss of signal is more likely to be caused by the formation of either $[CuOCu]^{2+}$ dimers with antiferromagnetic coupling between the two Cu, larger "Cu_xO_y" clusters, or 3-coordinate Cu in ZCuOH sites.[34,35] For samples with low Cu-loading, the decrease in signal is small or non-existent. For Cu-loading above 1 wt.%, a significant decrease in signal was observed by thermal activation, see Figure 3.

Ex-situ EPR spectra of fresh and thermally activated CuCHA

The EPR spectra of the fresh hydrated samples are very similar to spectra of previously measured CuCHA materials[27] and no clear differences between the OH- and NaOH route materials are observed. They are characterized by a broad featureless isotropic signal with a g-value at ~2.18 and an axial anisotropic spectrum typical for Cu^{2+} in a tetragonal coordination environment with oxygen atoms. See selected spectra in the upper part of Figure 4. The isotropic part of the spectra for the fresh samples is assigned to Cu^{2+} coordinated to water. The direction of the anisotropy axis of Cu changes fast on the timescale of the EPR experiment in the hydrated CuCHA due to mobility partially averaging out the anisotropy.[39] The amount of featureless isotropic signal is larger for samples with high Cu-load. The axial anisotropic part of the spectrum is identified by observation of two of the four expected hyperfine features in the low field part of the spectrum. They are, however, not coinciding with the parallel features observed after thermal activation of the samples, see Figure 4, bottom. This indicates that for this species Cu^{2+} is coordinated to one or more water

ChemCatChem

Research Article
doi.org/10.1002/cctc.202301377

**Chemistry
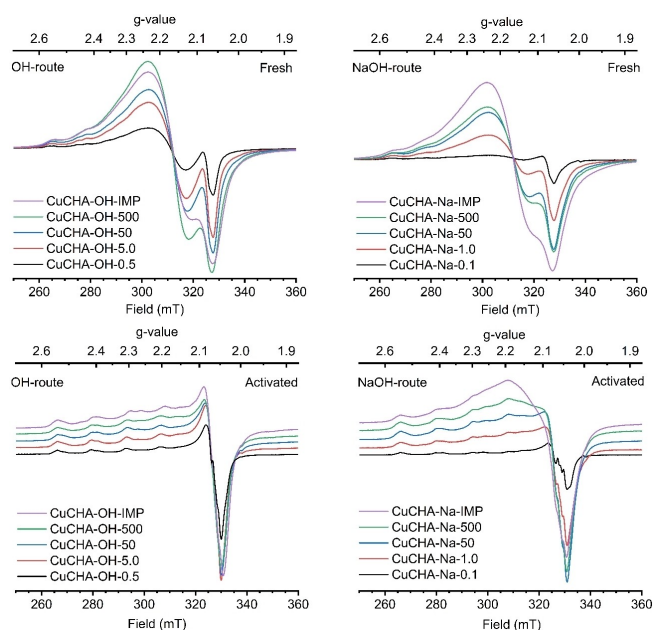Europe**
European Chemical
Societies Publishing

Figure 4. Background-corrected and normalized (by mass) EPR spectra measured at room temperature: Top: Fresh samples after calcination and several days' exposure to ambient conditions. Bottom: Thermally activated (250 °C in 10 % O_2 in He, 200 mL/min) samples after cooling to room temperature in a He flow.

molecules but it is immobilized and does not possess rotational freedom. The hyperfine features of the anisotropic species in the fresh samples are only well resolved for the materials with a low Cu load. For fresh CuCHA-OH-0.5 we determine $g_{\parallel} = 2.41$ and $A_{\parallel} = 370$ MHz. After thermal activation of the same sample, the dominant anisotropic Cu species has a significantly different set of parameters of $g_{\parallel} = 2.37$ and $A_{\parallel} = 430$ MHz.

In general, for samples with higher copper concentration, an increased linewidth of the EPR signal is observed. The effect is very visible in the high field part of the spectra. A similar observation has been noted by Feng Gao et al.[19] and can probably be explained by the increased level of paramagnetic exchange. For samples with the highest Cu content, an exchange narrowed EPR signal due to strong paramagnetic exchange is potentially also contributing. If this is the case, it will be impossible to distinguish this contribution from other isotropic contributions.

Upon applying a gas flow of 10 % O_2 in He at room temperature, the intensity of the isotropic signal decreases, and the intensity of the anisotropic signal increases. The total EPR signal intensity increases by 10–20 % for all samples. The reason for this increase is not clear, but we considered several effects: 1. A small amount of copper can change from an EPR inactive state to an EPR active state in the gentle drying process due to a decrease in the number of close Cu–Cu species. 2. The removal of free water molecules in the cages of the zeolite results in a slightly better critical coupling in the cavity (better Q-factor), less noise and an improved baseline. Both possibilities made us believe that the intensity of the spectrum after the stabilization is a better reference point for comparison with the

subsequent spectra of the in-situ measurements and it is therefore used as the reference point for determining relative EPR signal intensities.

The EPR spectra of CuCHA after the thermal activation are typical for Cu^{2+} and can be described by a parallel region (low field) and a perpendicular region (high field). The isotropic contribution largely disappeared since the fast motion of these Cu sites is lost along with the bound water molecules. After the thermal activation, all the observed EPR spectra have the characteristics of immobilized Cu^{2+} with approximate axial symmetry. The full EPR spectra for selected CuCHA catalysts are given in Figure S4. The zoom-in of the low-field region for four low concentration samples, CuCHA-HF-0.5, CuCHA-OH-0.5, CuCHA-Na-0.1, CuCHA-COM-0.1 are given in Figure 5, left and for three high-concentration samples, CuCHA-OH-IMP, CuCHA-Na-500, CuCHA-COM-50 in Figure 5, right. Previously published results from our group,[34] see Table 2, are discussed to compare with the new results.

The EPR spectra of CuCHA-COM samples has an extra feature close to $g = 2$ which is not assigned to Cu^{2+}. It is visible in the spectrum as a negative peak between 340 and 350 mT, see Figure S4. The feature changes intensity with temperature during in-situ measurements and our analysis of the relative intensity of the EPR signal for the commercial samples is significantly affected. Furthermore, a broad underlying signal with unresolved features causes a change in the baseline as the temperature changes. The combination of the position and temperature dependence of these two signals makes us assume that the signal is caused by an iron impurity in the parent zeolite. The presence of approximately 600 ppm iron was confirmed by XRF in the commercially available parent zeolite. Due to the temperature dependence, the baseline problems and the possible reactivity of the species giving the $g = 2$ signal with various reactant gases the quantification for this sample is unreliable, and the results from the in-situ measurements and the quantitative analysis of CuCHA based upon the commercial zeolite were discarded. The spectrum given in Figure 5 for CuCHA-COM reveals that the response for the dilute sample is very similar to that of CuCHA-OH.
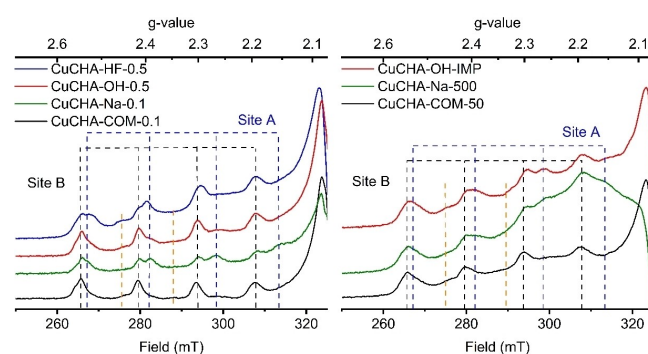

Figure 5. Zoom-in of the hyperfine coupling pattern in EPR spectra of CuCHA samples after thermal activation. The parent zeolites were synthesized by different synthesis routes with comparable Si/Al ratio. Left: Low Cu loading samples (0.1–0.8 wt.% Cu). Right: High Cu loading samples. The EPR spectra were all measured at room temperature in a flow of He.

ChemCatChem

Research Article
doi.org/10.1002/cctc.202301377

Chemistry Europe
European Chemical
Societies Publishing

The EPR spectrum of the dilute CuCHA-OH sample shows only one type of Cu signal, Site B. Dilute CuCHA-Na and CuCHA-HF samples show EPR spectra with significant contributions from both Site A and Site B. This is evident from the two low field peaks at ~268 mT and ~282 mT in Figure 5. The other two peaks in the hyperfine multiplet of Site A are less visible since the apparent intensities of the peaks decreases due to anisotropic line broadening (A- and g-strain). Furthermore, the close proximity of the large peak at g~2.06 shrouds the features. Besides Site A and B, the EPR spectra of all samples contain varying amounts of at least one extra EPR signal with a partially resolved hyperfine coupling pattern. These extra peaks are marked with orange in Figure 5 and were recently assigned as a 4-coordinate ZCuOH species.[35,40] The intensities of these extra signals increase with copper loading; they do, however, remain a minor contribution to the EPR signal and are not considered in the quantification described below.

Cu centers can be sampling several positions in the CHA cages at elevated temperatures due to thermal motion. This has been discussed in the context of the UV-Vis spectra of CuCHA.[41] It should be noted, that if the rate of change of Cu position or coordination sphere is faster than the frequency of EPR (more than 4 orders of magnitude lower than the frequency of visible light), the result is an EPR response which is in the fast motion regime: A sharp EPR signal corresponding to a spectrum with averaged spin Hamiltonian parameters. Only if the motion is slow compared to the EPR frequency will individual spectra from each position be observed. Little information on expected sampling rates can be found in the literature but considering the relatively simple and sharp signals usually observed, we expect this sampling rate to be above the EPR frequency of approximately 10^{10} Hz.

Some changes in the EPR spectra are observed when going from low to high loading. CuCHA from commercial CHA show only a minor change corresponding to a slightly higher relative amount of the Site A-species for the high Cu loading sample. The spectra of CuCHA-Na samples differ mainly in two ways: The relative intensities of Site A and Site C (the featureless isotropic signal centered at $g_{iso} = 2.15 \pm 0.01$) are considerably higher in the high loading sample. The g-value of Site C is the same as the averaged g-values for the EPR signal from the isolated Cu^{2+} ions in Site A and Site B but it is significantly

different from the one observed in the isotropic part of the fresh samples ($g_{iso} \approx 2.18$). We conclude that Site C does not come from hydrated Cu-species. Since CuCHA-Na samples has a larger proportion of extra-framework Al we hypothesize that at the high exchange level, more Cu ended up associated with the extra-framework Al. For the CuCHA-OH samples the proportion of Site A is also larger for higher Cu loadings but they do not show the same amount of isotropic signal as the CuCHA–Na samples with high Cu-loadings.

In-situ EPR during thermal activation

Just after the thermal activation at 250 °C, the intensities of the EPR spectra are lower for all samples compared to the fresh samples. Part of this intensity loss is due to the Boltzmann distribution of the two spin states since the EPR signal intensity is proportional to the population difference. In the high-temperature limit, this effect is approximated well by the ratio between the absolute temperatures. To compare spectra obtained at different temperatures directly, the intensity of the spectrum obtained at temperature T was corrected by multiplying with T/293 K. Even after correcting for this effect, the EPR signal intensity is consistently lower after thermal activation, see Table 4. The effect is more pronounced for high-loading samples.

The amount of EPR active Cu (in wt.% Cu) after thermal activation is calculated by multiplying the Boltzmann corrected relative EPR signal intensity after activation by the total wt.% of Cu on the fresh samples as determined by the EPR quantification experiments. This corresponds to multiplying the entries in the columns of Table 4 for each CHA material, see Figure 6 where the results are plotted as a function of the EPR active Cu in the fresh sample. The slope for the CuCHA-Na samples is steeper than that for the CuCHA-OH samples. Both impregnated samples (IMP) fall significantly below the fitted lines which means that an even higher amount of copper became EPR inactive in these samples after the thermal activation.

According to the literature, Z_2Cu sites are EPR active[19,27,34,42] after thermal activation and it is the consensus that these sites are preferentially occupied.[6,36,43] Some of the ZCuOH and all of the oligomeric Cu sites are EPR inactive[34,36] and are only

Table 4. Amount of EPR active Cu in CuCHA samples from the OH- and NaOH-route. For fresh samples, the amount of EPR active Cu is given as wt.% Cu and has been determined by quantification the of background corrected EPR spectra of fresh samples using a calibration curve constructed using Cu reference samples. For the thermally activated samples, the result is given as the relative intensity of the EPR signal compared to the intensity of the fresh sample. The results for thermally activated samples were Boltzmann corrected to room temperature.

| Sample | OH-route CHA | | Sample | NaOH-route CHA | |
	EPR active Cu, fresh [wt.%]	EPR active Cu, therm. act. I/I_{fresh}		EPR active Cu, fresh [wt.%]	EPR active Cu, therm. act. I/I_{fresh}
CuCHA-OH-0.5	0.5	92%	CuCHA-Na-0.1	0.1	101%
CuCHA-OH-5	1.0	75%	CuCHA-Na-1	0.8	103%
CuCHA-OH-50	1.5	70%	CuCHA-Na-50	1.4	91%
CuCHA-OH-500	2.5	68%	CuCHA-Na-500	1.7	84%
CuCHA-OH-IMP	2.3	52%	CuCHA-Na-IMP	1.9	73%

ChemCatChem

Research Article
doi.org/10.1002/cctc.202301377

Chemistry Europe
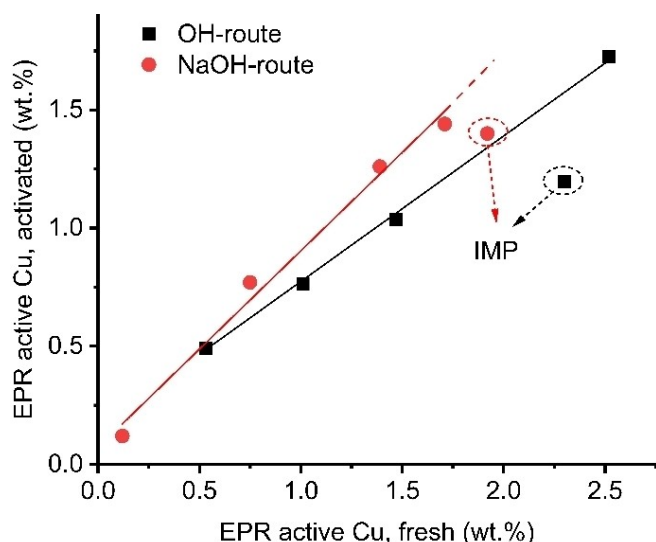European Chemical
Societies Publishing

Figure 6. EPR active Cu in the activated samples vs. EPR active Cu in the fresh samples shown as weight percent Cu of the samples. CuCHA samples with NaOH-route CHA are given as red circles. CuCHA samples with OH-route CHA are given as black squares.

occupied after the more stable Z_2Cu sites are filled. It was previously observed by EPR that the occupation develops somewhat gradual when increasing the Cu loading[35] and the results presented here confirm this.

Intensities of EPR spectra during SCR relevant gas exposure

CuCHA samples exposed to $NO + NH_3$ at 200 °C lose most of the EPR signal intensity due to paramagnetic Cu^{2+} being reduced to diamagnetic Cu^+ which is EPR inactive. When exposed to $NO + O_2$, Cu^+ oxidizes to Cu^{2+}, causing the EPR signal to be restored. The change in intensity of the EPR signal relative to the first spectrum in the fresh samples provides the possibility to probe the extent to which EPR active Cu participates in the redox reaction. We have previously observed a correlation between the size of the "redox window" defined in Eq. 2 and the activity of the catalyst in the SCR reaction.[44,45]

$$\Delta EPR \text{ active Cu, } ox - red = \frac{I_{ox} - I_{red}}{I_{fresh}} \cdot$$

EPR active Cu, fresh   (2)

Here I_{ox} is the intensity of the EPR spectrum after $NO + O_2$ exposure at 200 °C, I_{red} is the intensity of the EPR spectrum after exposure to $NO + NH_3$ at 200 °C, I_{fresh} is the intensity of the EPR spectrum of the fresh sample in 10 % O_2 flow, and "EPR active Cu, fresh" is the amount of Cu in wt.% of the fresh sample as determined by quantification by EPR.

For any Cu to be catalytically active it must be able to change oxidation states between Cu^+ and Cu^{2+}. All Cu^+ will be EPR inactive due to Cu^+ being diamagnetic. Cu^{2+} can, in principle, be both EPR active and EPR inactive. Thus, it is not expected that EPR will necessarily probe the full extent to which

Cu can change oxidation state under the given conditions. Fortunately, NH_3 forms strong bonds to Cu^{2+} and the presence of NH_3 during the SCR reactions lessens the loss of signal due to both clustering of Cu and low-coordinate Cu species. We predict that the quantification of Cu^{2+} is quite secure when NH_3 is present in excess. As mentioned above, our quantification method slightly overestimates the EPR active Cu content. With these assumptions and small reservations, the redox window of selected CuCHA synthesized by the NaOH-route and the OH-route has been determined, see Figure 7.

The results in Figure 7 show that samples with a high Cu content also have more Cu that is responsive to the change in reaction gases as measured by EPR. The linear fits in Figure 7 have a slope of 0.83 for the OH-route CuCHA and 0.62 for the NaOH-route CuCHA. We conclude that the size of the redox window increases with the amount of EPR active Cu for all samples, but that the increase in the redox window is not 1:1. For the same amount of EPR active Cu in the fresh samples, less copper participated in the redox reaction for NaOH-route CuCHA samples. The samples prepared by impregnation fall on the fitted lines in Figure 7, but not in Figure 6. When CuCHA is reduced with NO and NH_3, Cu gains high mobility in the zeolite framework as $[Cu(NH_3)_2]^+$ and thus after the reduction/oxidation treatment, all Cu finds its way to the equilibrium positions.[46] The thermal activation procedure alone is not sufficient to achieve this.

Quantification of copper distribution in NaOH- and OH-route CuCHA

EPR signal intensities are obtained by double integration of the EPR spectra after background correction. Three different types of experiments are analyzed in the following: 1. Ex-situ investigations to quantify all the EPR active copper in the fresh Cu-CHA. 2. In-situ thermal activation to quantify the amount of EPR inactive copper species and to quantify the amount of Site
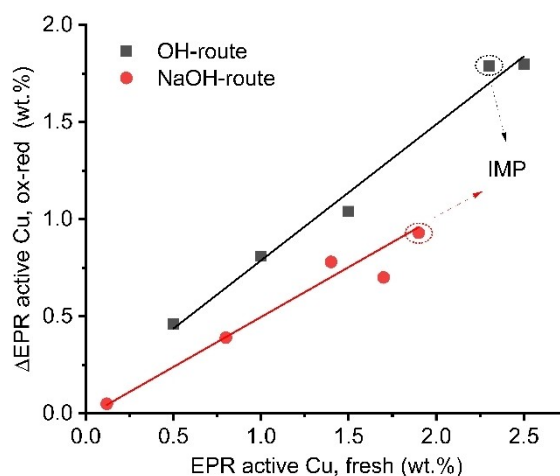

Figure 7. The change in EPR active Cu (in wt.%) at 200 °C during cycling between reducing conditions (1000 ppm of both NO and NH_3) and oxidizing conditions (1000 ppm of NO and 10 % of O_2) of the CuCHA samples. The lines represent linear fits of the data points.

ChemCatChem

Research Article
doi.org/10.1002/cctc.202301377

**Chemistry
Europe**
European Chemical
Societies Publishing

A, B and C by EPR spectral simulation. 3. In-situ redox cycle measurements to quantify the redox active copper in zeolites. The EPR spectra after thermal activation are simulated using the simplified spin Hamiltonian given in Eq. 1. The simulated spectra were fitted to the experimental spectrum, using the EasySpin software package as described in the experimental section. Spin Hamiltonian parameters obtained from the simulation are given in Table 5.

Figure 8 depicts the copper distribution according to the simulation of the Cu EPR spectra in OH-route and NaOH-route samples. The total height of the columns indicates the quantification of EPR signal of the fresh samples obtained by double integration of the spectra. The heights of columns without the part marked "EPR inactive" indicate the quantification of the EPR signal after the applied protocol. The columns in red nuances are partitioned according to speciation of the Cu signal at room temperature after the thermal activation pretreatment as Site A, B, C or "EPR inactive". The columns in blue nuances are partitioned according to behavior under reduction in $NO+NH_3$ and oxidation in $NO+O_2$ at 200°C as "Always oxidized", "Redox active" or "EPR inactive".

Several observations can be made from the data. The OH-route CHA has a higher maximal capacity for ion exchanged Cu but CuCHA-OH samples also lose more EPR signal intensity upon thermal activation and ends up with a total signal intensity which is similar to that of the CuCHA-Na samples. During the treatment with SCR gases some of the Cu becomes observable again and the amount of Cu observed on the fresh samples and on the oxidized samples are almost the same within the uncertainty. After the reduction-oxidation treatment with SCR gases, the fully exchanged samples CuCHA-OH-500 and CuCHA-Na-500 behaved almost the same as the corresponding impregnated samples according to EPR even though

the impregnated samples contained more than twice as much Cu.

$^{15}NH_3$ exchange at 100°C

The exposure of a CuCHA-HF sample to NH_3 was described previously.[42] At 200°C the ligand exchange is in general too fast to follow and therefore the experiments were performed at a lower temperature. Analysis of the hyperfine coupling patterns and the super hyperfine patterns visible in the EPR spectra shows that Cu^{2+} changes from being coordinated to the framework oxygen atoms to being coordinated to the nitrogen atoms of the NH_3 molecules. The rate is identical to the rate of NH_3 reaching the sample.[36,42] The change in coordination is observed by the disappearance of parallel features belonging to Site A and Site B and the appearance of features belonging to $[Cu(NH_3)_x]^{2+}$ (x=3,4 or 5) at $g_\parallel = 2.26$ and $A_\parallel = 550$ MHz. Furthermore, the axial part of the spectrum shows superhyperfine coupling after exposure to NH_3, see the features at ~320 mT to 340 mT in Figure 6.

To investigate the interaction between NH_3 and the EPR active Cu^{2+} centers further, we exposed a CuCHA-HF sample with Cu content of 0.2 wt.% Cu to isotope-labeled $^{15}NH_3$ at 100°C. ^{15}N has the nuclear spin $I=\frac{1}{2}$ and ^{14}N has $I=1$, therefore the number of superhyperfine lines in EPR resulting from the interaction of the unpaired electron with the nuclei will be different for e.g. $[Cu(^{14}NH_3)_4]^{2+}$ and for $[Cu(^{15}NH_3)_4]^{2+}$. We produced $^{15}NH_3$ in-situ from a solid-state reaction between $^{15}NH_4Cl$ and KOH: When mixed, the two salts form $^{15}NH_3$, KCl, and H_2O. A reaction tube with $^{15}NH_4Cl$ and one with KOH were connected in a closed system and flushed with He. The two solids were mixed and stirred under He for a few minutes and then He gas was slowly led through the system and passed through the sample kept at 100°C in the EPR cavity. The CuCHA was left to equilibrate in the $^{15}NH_3$-containing gas for 20 minutes, flushed shortly with He and then natural abundance NH_3 (500 ppm in He, 99.6% ^{14}N) was led over the sample.

The black spectrum in Figure 9 was recorded at 100°C after exposure to $^{15}NH_3$. Based on the hyperfine coupling pattern in this spectrum, it is likely that the sample was not fully saturated with NH_3 since the four peaks are slightly shifted towards low field. After the subsequent exposure to 500 ppm NH_3, the EPR spectrum changed to the normal $[Cu(^{14}NH_3)_4]^{2+}$ spectrum (red in Figure 9) and the intermediate spectra show that the reaction was essentially complete already after 4 minutes. This is strong evidence that the NH_3 coordinated Cu species on these samples exhibited fast ligand exchange.

Table 5. Spin Hamiltonian parameters obtained from the simulation of CuCHA EPR spectra measured at room temperature in a flow of He after thermal activation in O_2/He at 250°C.

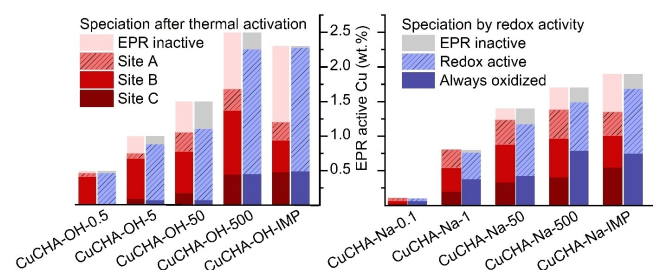| Site A			Site B			Site C
$A_\parallel$ [MHz]	$g_\parallel$	$g_\perp$	$A_\parallel$ [MHz]	$g_\parallel$	$g_\perp$	g_{iso}
490	2.328	2.06	456	2.358	2.07	2.15

Figure 8. Speciation according to the EPR investigations. Left: CuCHA-OH samples. Right: CuCHA-Na samples. For each sample, the Cu species are distributed according to the room temperature EPR spectra after a thermal activation at 250°C in the left stacked columns (red colors) and according to their behavior during in-situ EPR at 200°C when exposed to reducing (NO $+NH_3$) gas or oxidizing gas ($NO+O_2$) in the right stacked columns (blue colors).

Discussion

It is important to be aware of differences in otherwise similar materials and our analysis of CuCHA from different synthesis methods reveals the complexity that affects the activity and speciation of Cu in the materials. The observed differences in crystal shapes and sizes by the TEM imaging further underlines
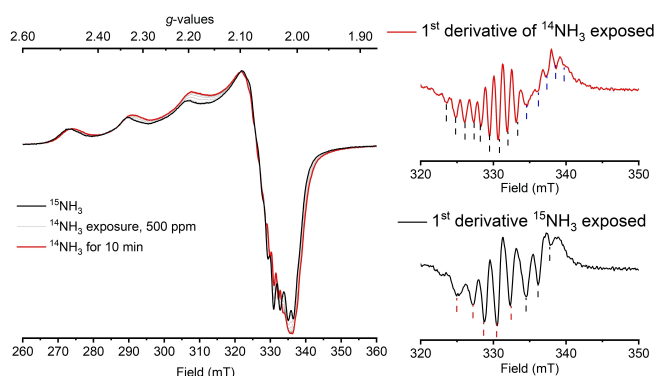
ChemCatChem

Research Article
doi.org/10.1002/cctc.202301377

**Chemistry
Europe**

European Chemical
Societies Publishing

Figure 9. Background corrected EPR spectra of CuCHA-HF with 0.2 wt.% Cu exposed to NH_3. The black spectrum was measured in a flow of pure He just after the sample had been exposed to $^{15}NH_3$. The red spectrum was measured after the sample had been flushed with 500 ppm NH_3 (99.6% ^{14}N) at 100 °C for 10 minutes. Intermediate spectra every 45 seconds are shown in grey. To the right is the derivative of the red and black spectra in the range 320–350 mT. Dashed lines are inserted as a visual aids.

this. Materials may be physically different in crystal size, shape, and nature of defects even if prepared by the same synthesis method. If the method of synthesis is different, the materials can differ even more. The influence of such differences should not be ignored when comparing the result of analysis by different research groups.

All the Cu sites in the investigated materials are EPR active in the hydrated fresh state and can be classified according to the room temperature EPR spectra after a thermal activation in a dry O_2/He mixture as belonging to Site A, B, C or EPR inactive. For Site A and B, the observed spectra and spin Hamiltonian values provided strong evidence for a Cu^{2+} species with 4O coordination and this is also a reasonable suggestion for Site C. Independently, we also classify all Cu in the samples in 3 classes according to the behavior regarding reduction and oxidation with SCR gasses. In the following we will go deeper into the data by comparing the spectra and the quantification of Cu between samples.

As observed in Figure 5, there is a difference in the amount of Site A between the different sample series: For the commercial CHA, Site A contributes only a little to the EPR signal in both the dilute and concentrated sample; in diluted CuCHA-OH the contribution of Site A is small but in the concentrated sample it is much larger; in both diluted and concentrated CuCHA-Na samples the contributions are large.

According to our analysis, Cu species with a Site B-type EPR spectrum is easily reduced by $NO+NH_3$ in all samples. Cu species with a Site A-type EPR spectrum, however, differs between samples. A considerable amount of Site A in the CuCHA-Na samples is not reduced but all of Site A in CuCHA-OH samples is reduced by $NO+NH_3$, see Figs. 10 and S5. Previous research from our group demonstrated that Cu assigned to both Site A and B in a HF-route CuCHA are easily reduced.[42] This suggested to us that the EPR spectrum assigned as Site A is due to chemically different Cu species that have different reactivity towards NO and NH_3 and that it depends on the synthesis method of the CHA which one is

formed. These two types of Site A has the same set of parallel spin Hamiltonian parameters, and therefore EPR cannot distinguish them. Another observation from the previous work is that for the HF-route CuCHA, oxidation with $NO+O_2$ results in the EPR signal from Site A appearing first whereas Site B appears slightly later. To check for this type of behavior, several spectra were analyzed, see Figure 10. The initial oxidation rate in $NO+O_2$ is fast compared to our time resolution so to detect this effect, we calculate a difference spectrum between the first spectrum after addition of the oxidizing mixture and a later one. The difference spectra in Figure 10 are multiplied with 2 and 4, respectively to blow up the details in the parallel hyperfine features. The difference spectra are assigned to Site A for both samples in accordance with the results for the HF-route CuCHA. We conclude that the very first Cu being oxidized in this way gives a spectrum of the Site A type for CuCHA from all three synthesis methods.

In conclusion, Site A should be further differentiated for CuCHA–Na samples according to the reactivity. It was suggested previously that Site A and B differ in the distribution of Al in the 6-membered ring giving the two different types of Z_2Cu[27,36] and this may still be true in some CHA materials, but for Cu in this particular CuCHA–Na material some Cu sites give the same type of EPR signal but has different reactivity. It is highly likely that the unreducible Site A-type Cu differs more fundamentally from Site B than just by the siting of 2 Al in a 6mr. The addition of Na^+ during the CHA synthesis affects the ion-exchange sites and therefore the distribution of Cu in the ion-exchanged material. Considering the amount of Al in non-ideal sites or extra framework positions, we also considered if obstruction of gas flow to some sites plays a role. Since all of Cu in Site B reduces easily and since the channel structure in CHA is 3-dimensional and not easily blocked, we discarded this hypothesis.

Cu assigned to Site B is redox active for all 10 CuCHA-OH and CuCHA-Na samples. For the highly loaded CuCHA-OH samples, the total amount of redox active Cu is significantly higher than the amount of Site B. Looking at the quantification in Figure 8, we arrive at the conclusion that most of the Cu which is EPR inactive after thermal activation must contribute
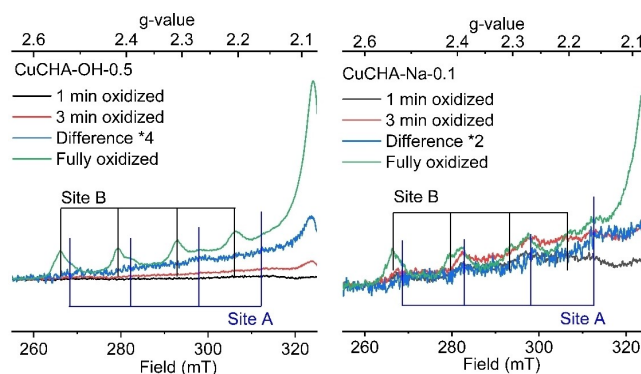

Figure 10. Selected spectra during oxidation by $NO+O_2$. The difference spectra were calculated between spectra obtained after 3 and 1 minute of oxidation.

to the redox active Cu. This was also the case in ref. [35]. For the CuCHA-OH samples, the contribution is quite substantial, for CuCHA-Na samples the contribution is smaller in accordance with the lower amount of EPR inactive Cu after thermal activation. For the CuCHA-OH samples, the amount of unreducible Cu (denoted "Always oxidized" in Figure 8) correlates well with the amount of Site C. The remaining spectrum after reduction has the broad features of Site C confirming this interpretation. On the other hand, for the CuCHA-Na samples, parts of both Site C and Site A were unreducible. To sum up, Site B and a significant amount of the EPR inactive Cu are redox active for both series of CuCHA, Site A is redox active for CuCHA-OH samples, but most of Site A is not redox active for CuCHA-Na samples. Site C is always oxidized for CuCHA-OH samples, but is not as clearly assigned for CuCHA-Na.

According to the NMR and XRF results the CuCHA-Na material has a significant amount of tetrahedrally coordinated Al[47] which is not in the normal CHA-framework T-site, see Figure S1. This type of Al is different from the extra-framework Al normally found around a chemical shift of 1 ppm in ^{27}Al solid state NMR. Bokhoven and co-workers proposed a new term "framework-associated Al" to distinguish these two types of non-ideal Al positions.[48] The framework-associated Al may be related to the extra peak in the XRD diffractogram for CHA-Na. CuCHA-OH on the other hand has only a minor amount of extra-framework Al and none of the framework-associated Al. Cu bound at the normal extra-framework Al is expected to give a broad featureless EPR spectrum and thus to be found as Site C. By comparing data for CuCHA-OH and CuCHA-Na in Figure 8 we tentatively assign Cu close to framework-associated Al in the CuCHA-Na sample to the "Always oxidized" Cu with the Site A type EPR spectrum. The arguments for our assignment are as follows: Cu close to extra-framework Al is expected to behave similarly in the two different sample series. Since it exhibits the Site C type EPR spectrum in the CuCHA-OH series, it should also be the case in the CuCHA-Na series. The ideal Z_2Cu sites give the Site B EPR spectrum in both series. The quantification of the Site B and Site C EPR spectra are reasonable given this interpretation. Cu close to the framework-associated Al and Cu in the "Always oxidized"-type of Site A are both present in the CuCHA-Na samples and not in the CuCHA-OH samples. The amount of framework associated Al is quite substantial according to the ^{27}Al SS-NMR spectrum in Figure S1 and therefore, we also expect a substantial amount of Cu close to this Al. The amount of "EPR inactive" Cu is quite modest and cannot account for Cu close to framework associated Cu. It is more reasonable to suggest that Cu close to the framework associated Al is the "Always oxidized" Cu having a Site A-type EPR spectrum.

The connection between the Cu sites observable by EPR and the different catalytically active sites is still under discussion. Our results as well as results presented by other groups show that the first Cu introduced into the material are found in stable, well-defined, redox active and catalytically active sites giving the EPR spectrum of Site B. These sites have a coordination sphere of 4 oxygens in a 6mr of the framework with 2 Al, Z_2Cu. According to recent investigations of a sample

with a very small amount of Cu where the application of more advanced EPR methods is possible, the two Al T-sites are most likely in the "para" position in the 6mr.[39]

Site A, on the other hand, is more difficult to assign to a specific Cu site. The amount of Site A differs significantly depending on the synthesis method, see Figure 5 and Table 2. For CHA materials with few defect sites, Site A is suggested to be the "meta" type of Z_2Cu site. They are also catalytically active and are the first ones found after reoxidation.[42] For CuCHA-Na with more extra-framework Al and an additional shoulder on the SS-NMR peak for the Al T-site, we find Cu, which gives a Site A type EPR spectrum, but has different reactivity. This duality, which is so far only found for the NaOH-route CHA, is suspected to be the reason for some of the confusion in the literature. For perfect CHA zeolites without non-ideal Al sites of either type, the amount of "Always oxidized" Site A is negligible.

The ZCuOH sites are normally considered the most catalytically active sites at low temperatures since they have less strong interactions with the framework, and they can therefore more easily be solvated by ammonia and activate dioxygen forming a peroxo-bridged dimer in the oxidation half-cycle of the SCR reaction.[9] ZCuOH does not belong to neither Site A nor Site B, but can be found in some samples at low temperature with a signature set of parallel EPR peaks.[35,40] At higher temperatures or in samples with higher Cu content and less resolution, ZCuOH can be found either as the EPR inactive Cu if they are 3-coordinate or as part of Site C, if they are 4-coordinate and therefore EPR active but the parallel EPR peaks are not recognizable due to line broadening.[35] Cu in ZCuOH type sites is expected to be EPR active after exposure to NH_3 and to be redox active.

We observed in the isotope-labeling experiment that Cu preferred coordination to NH_3 in the CHA cage rather than framework oxygen in agreement with the literature[37] and that coordinated NH_3 exchanges fast with gas phase NH_3. To our knowledge, no one has probed the ability of the Cu centers to exchange the ligands as shown in this work by in-situ EPR. The results demonstrate that the CuCHA system is highly dynamic even at a relatively low temperature of 100 °C.

Conclusions

CuCHA samples were successfully synthesized with and without Na^+ present in the synthesis gel. It was observed by TEM imaging that the products had different morphologies. By NMR and XRF it was determined that the CHA zeolite synthesized by the NaOH-method contained a considerable amount of extra-framework Al and framework-associated Al and thus was not a perfect material, but probably very representative of materials investigated in the literature. The EPR investigation provided two types of differentiation between Cu sites. One based on the EPR spectra after thermal activation in a dry oxygen flow at 250 °C and one based upon the intensity of the EPR signal after exposure to a mixture of SCR gases. The investigation showed that for all samples, Site B Cu was both stable and highly redox active. Cu associated with extra-framework or associated-frame-

ChemCatChem

Research Article
doi.org/10.1002/cctc.202301377

Chemistry
Europe

European Chemical
Societies Publishing

work Al, on the other hand was not redox active and therefore also not catalytically active.

The maximum amount of redox active Cu and thus the redox window was larger for the CuCHA-OH samples compared to the CuCHA-Na samples due to the higher ion-exchange capability of the parent zeolite and the higher number of reducible sites. A large part of the Cu present was not observable by EPR in the thermally activated sample but could be observed after a reduction and oxidation protocol with SCR relevant gases.

Some Cu was assigned to Site A in all samples, and it was also shown that the most reactive Cu towards oxidation belonged to Site A for both CuCHA from the OH- and NaOH route in accordance with previous work on CuCHA from the HF-route. For our NaOH-route CuCHA, however, the total amount of Cu assigned to Site A after thermal activation was much larger than for the others and most of it was in fact not redox active. We concluded that for our NaOH-route CuCHA, two different Cu sites were assigned to Site A. They were shown by the redox experiments to be different.

The preference for NH_3 coordination over framework O was shown by exposure to NH_3 in accordance with observations from the literature.[9,36,37] The system was shown to be very labile at 100 °C since $^{15}NH_3$ coordinated Cu is completely exchanged to $^{14}NH_3$ within 10 min exposure to 500 ppm $^{14}NH_3$.

In conclusion, in-situ EPR was used to investigate the Cu distribution directly and to investigate the Al distribution indirectly for CuCHA zeolites. The presence of additional ions besides the structural directing agent was proven to influence the Al-distribution and hence the Cu speciation and the redox window in the resulting CuCHA material. To obtain more of the attractive Site B copper species, The effort should be directed towards synthesizing CHA zeolites with a large amount of paired Al sites and a small amount of extra-framework and framework-associated Al.

Experimental

Synthesis of CHA materials

The synthesis of CHA by the NaOH route was performed similarly to the method described by Gounder et al.,[14] which is modified from the original method described by Zones.[13]

NaOH-route: 24.839 g of TMAdaOH (30 mmol, *N,N,N*-trimethyl-1-adamantylammonium hydroxide 25 % in H_2O, Sachem), was added to a Teflon beaker containing 2.243 g water (18.2 MΩ·cm) and 0.583 g NaOH (15 mmol, sodium hydroxide, Sigma Aldrich, 98 %). 0.856 g Al-*i*-Pr (4 mmol, aluminum iso-propoxide, Sigma Aldrich, 99.99 %) was added and dissolved by stirring for 30 min at 40 °C. The clear solution was cooled to room temperature; 12.507 g TEOS (60 mmol, tetraethylorthosilicate, Sigma Aldrich, ≥ 99 %) was added; the mixture was stirred for 1 h and the resulting gel-like substance was transferred to a Teflon lined autoclave. The autoclave was left in an oven for 6 days at 150 °C; the resulting white crystals were washed 10 times with 40 mL deionized water and separated by centrifuge at 3900 rpm. When the washing water was pH-neutral, the zeolite was dried overnight at 90 °C and calcined for 3 h at 580 °C. The Na$^+$:SDA ratio was 0.5 in the NaOH-route synthesis gel

and the gel had Si/Al = 14. The final product was a white crystalline powder which was measured by X-ray fluorescence (XRF) to have Si/Al = 6 and by solid state NMR to have Si/Al = 8.4.

OH-route: The synthesis was analogous to described for the NaOH-route omitting the addition of NaOH: Na$^+$:SDA = 0. The resulting white crystalline powder was measured by XRF to have Si/Al = 11.3 and by NMR to have Si/Al = 13.2.

A previously synthesized CHA prepared using the HF-method with Si/Al = 15[23] was used in order to compare the previous results directly with the results obtained on new materials.

Commercially available NH_4-SSZ-13 was purchased (ACSmaterial) with a Si/Al = 10–15, Na_2O < 500 ppm, surface area determined by BET: ~671 m^2/g. This material was made by the hydrothermal method and was calcined at 580 °C for 5 h before use.

Ion exchange: 3 g of the calcined Na-CHA was ion-exchanged with 500 mL of an NH_4NO_3 solution (4 M, Aldrich) by stirring overnight, washed 3 times with deionized water, and calcined as in the previous step to obtain the H-CHA form. The as-prepared H-CHA was divided into batches for ion exchange with copper. To synthesize the four CuCHA–Na samples, the individual batches were ion-exchanged with 200 mL of 0.1, 1.0, 50.0, and 500 mM $Cu(NO_3)_2 \cdot 3H_2O$ (Sigma Aldrich, > 99 %) per gram of zeolite. To synthesize the four CuCHA-OH samples, H-CHA prepared by the OH-route were ion-exchanged with 200 mL of 0.5, 5.0, 50.0 and 500 mM $Cu(NO_3)_2 \cdot 3H_2O$ (Sigma Aldrich, > 99 %) per gram of zeolite. The ion exchange with Cu was in all cases obtained by stirring at room temperature for 15–18 h. The batches with 500 mM Cu^{2+} were stirred for 48 h total, to ensure the maximal uptake of copper. After ion-exchange the zeolite materials were washed 3 times with 33 mL deionized water; then dried at 90 °C overnight and finally calcined at 580 °C for 5 h.

HF-route H-CHA was ion-exchanged by 5 mM $Cu(NO_3)_2 \cdot 3H_2O$ (Riedel-de Haën, > 98 %) solution using 150 mL/g CHA.

Commercial H-CHA was ion-exchanged by adding an excess of aqueous solutions with 0.5 mM and 50 mM $Cu(NO_3)_2 \cdot 3H_2O$ (Sigma Aldrich, > 99 %) using~170 mL/g CHA and calcined at 580 °C for 5 h.

Impregnation: Impregnation of copper on H-form CHA from both OH-route and NaOH-route was performed by adding 15 mg $Cu(NO_3)_2 \cdot 3H_2O$ (Sigma Aldrich, > 99 %) in 20 mL of H_2O to 96 mg zeolite. The mixture was stirred and heated to 90 °C for 3 h until all water was evaporated. The resulting materials containing 4 wt.% Cu were dried for 5 h at 120 °C and calcined at 580 °C for 5 h.

Characterization

Powder X-Ray diffraction patterns were recorded on a Huber G670 using CuKα source using the transmission configuration. XRD was measured with a total exposure time of 1 hour from 3–100° 2θ with a resolution of 0.005°. A few mg of powdered sample was placed in a sample holder held in place by scotch tape. A background diffractogram of the sample holder with tape was collected and subtracted from the reported diffractograms.

X-Ray Fluorescence spectroscopy was measured using a PANanalytical Epsilon 3X on powdered samples with no pretreatment. The Si/Al-ratio was determined by comparing the result of representative Cu-exchanged zeolite samples with CHA zeolite standard samples with known Si/Al confirmed by Inductively Coupled Plasma – Optical Emission Spectroscopy (ICP-OES).

The Cu content of selected samples was determined by ICP-OES. The CuCHA samples were heated to 110 °C in aqua regia (50 mg/10 mL) and stirred for 1 h, cooled to RT, filtered through a syringe

filter, and diluted in 2 wt.% HNO_3. Standards were prepared by diluting a Cu ICP standard (1000 ppm $\pm$ 2 ppm, ISO 17025 and ISO Guide 34, Sigma-Aldrich) in 2 wt.% HNO_3.

The crystalline powders of CuCHA were imaged in an FEI Tecnai T20 G2 microscope at 200 keV. Before imaging, the sample was dispersed on a carbon grid.

Solid-state ^{29}Si NMR and ^{27}Al NMR were measured on a Bruker Advance III HD 14.05 T, using a 4 mm CP/MAS BBFO probe.

EPR spectra were obtained on an X-band continuous wave Bruker EMX spectrometer fitted with an ER 4102ST cavity. The spectra were typically measured at a microwave frequency of 9.46 GHz, microwave power of 6.67 mW. The magnetic field varied from 220 mT to 400 mT with a modulation frequency of 100 kHz and modulation amplitude of 5.2 G. In-situ experiments were performed as described in. [34]

Simulation and data treatment were performed in the EasySpin v. 5.2.28 package for Matlab R2019a.[49]

In-situ EPR spectra were recorded during thermal activation (also described as dehydration) in 10% O_2 in He for one hour at 250 °C. The thermal activation was followed by cooling to 200 °C and exposure to SCR-relevant gases. Selected samples were exposed to 1000 ppm NH_3 + 1000 ppm NO in balance He to reduce accessible Cu^{2+} species to Cu^+ and exposure to 1000 ppm NO + 10% O_2 to oxidize Cu^+ species to Cu^{2+}. Selected samples were also exposed to a mixture of 1000 ppm NH_3 + 1000 ppm NO + 10% O_2 to simulate an SCR environment.

Conflict of Interests

The authors declare no conflict of interest.

Data Availability Statement

The data that support the findings of this study are available from the corresponding author upon reasonable request.

[1] European Commission, *Report from the Commission to the European Parliament, the Council, the European Economic and Social Committee and the Committee of the Regions the Second Clean Air Out-Look*, COM(2021) 3, Brussels, **2021**.

[2] European Parliament and the Council of the European Union, *Official journal of the European Union* **2009**, *L188*, 1–13.

[3] I. Bull, U. Müller, *Process for the Direct Synthesis of Cu Containing Silicoaluminophosphate (Cu-SAPO-34)* **2011**, US2011076229 A1.

[4] C. Negri, T. Selleri, E. Borfecchia, A. Martini, K. A. Lomachenko, T. V. W. Janssens, M. Cutini, S. Bordiga, G. Berlier, *J. Am. Chem. Soc.* **2020**, *142*, 15884–15896.

[5] E. Borfecchia, K. A. Lomachenko, F. Giordanino, H. Falsig, P. Beato, A. V. Soldatov, S. Bordiga, C. Lamberti, *Chem. Sci.* **2015**, *6*, 548–563.

[6] C. Paolucci, A. A. Parekh, I. Khurana, J. R. Di Iorio, H. Li, J. D. Albarracin Caballero, A. J. Shih, T. Anggara, W. N. Delgass, J. T. Miller, F. H. Ribeiro, R. Gounder, W. F. Schneider, *J. Am. Chem. Soc.* **2016**, *138*, 6028–6048.

[7] T. V. W. Janssens, H. Falsig, L. F. Lundegaard, P. N. R. Vennestrøm, S. B. Rasmussen, P. G. Moses, F. Giordanino, E. Borfecchia, K. A. Lomachenko, C. Lamberti, S. Bordiga, A. Godiksen, S. Mossin, P. Beato, *ACS Catal.* **2015**, *5*, 2832–2845.

[8] T. Günter, H. Carvalho, D. E. Doronkin, T. Sheppard, P. Glatzel, A. J. Atkins, J. Rudolph, C. R. Jacob, M. Casapu, J.-D. Grunwaldt, *Chem. Commun.* **2015**, *51*, 9227–9230.

[9] C. Paolucci, I. Khurana, A. A. Parekh, S. Li, A. J. Shih, H. Li, J. R. Di Iorio, J. D. Albarracin-Caballero, A. Yezerets, J. T. Miller, W. N. Delgass, F. H. Ribeiro, W. F. Schneider, R. Gounder, *Science (1979)* **2017**, *357*, 898–903.

[10] F. Gao, E. D. Walter, M. Kollar, Y. Wang, J. Szanyi, C. H. F. Peden, *J. Catal.* **2014**, *319*, 1–14.

[11] A. R. Fahami, T. Günter, D. E. Doronkin, M. Casapu, D. Zengel, T. H. Vuong, M. Simon, F. Breher, A. V Kucherov, A. Brückner, J. D. Grunwaldt, *React. Chem. Eng.* **2019**, *4*, 1000–1018.

[12] C. Paolucci, J. R. Di Iorio, F. H. Ribeiro, R. Gounder, W. F. Schneider, in *Adv. Catal.*, Academic Press, **2016**, pp. 1–107.

[13] S. I. Zones, *Zeolite SSZ-13 and Its Method of Preparation* **1985**, US4544538 A.

[14] J. R. Di Iorio, R. Gounder, *Chem. Mater.* **2016**, *28*, 2236–2247.

[15] C. F. Macrae, I. Sovago, S. J. Cottrell, P. T. A. Galek, P. McCabe, E. Pidcock, M. Platings, G. P. Shields, J. S. Stevens, M. Towler, P. A. Wood, *J. Appl. Crystallogr.* **2020**, *53*, 226–235.

[16] C. Baerlocher, L. B. McCusker, D. H. Olson, *Atlas of Zeolite Framework Types*, Elsevier, Amsterdam, **2007**, p. 96.

[17] C. McCusker, L. B. Baerlocher, "http://www.iza-structure.org/databases," **2017**.

[18] W. Loewenstein, *Am. Mineral.* **1954**, *39*, 92–96.

[19] Y. Zhang, Y. Peng, J. Li, K. Groden, J. S. McEwen, E. D. Walter, Y. Chen, Y. Wang, F. Gao, *ACS Catal.* **2020**, *10*, 9410–9419.

[20] J. Luo, F. Gao, K. Kamasamudram, N. Currier, C. H. F. Peden, A. Yezerets, *J. Catal.* **2017**, *348*, 291–299.

[21] Y. Cui, Y. Wang, D. Mei, E. D. Walter, N. M. Washton, J. D. Holladay, Y. Wang, J. Szanyi, C. H. F. Peden, F. Gao, *J. Catal.* **2019**, *378*, 363–375.

[22] J. R. Di Iorio, S. Li, C. B. Jones, C. T. Nimlos, Y. Wang, E. Kunkes, V. Vattipalli, S. Prasad, A. Moini, W. F. Schneider, R. Gounder, *J. Am. Chem. Soc.* **2020**, *142*, 4807–4819.

[23] F. Giordanino, P. N. R. Vennestrøm, L. F. Lundegaard, F. N. Stappen, S. Mossin, P. Beato, S. Bordiga, C. Lamberti, *Dalton Trans.* **2013**, *42*, 12741–12761, DOI 10.1039/c3dt50732g.

[24] E. A. Eilertsen, B. Arstad, S. Svelle, K. P. Lillerud, *Microporous Mesoporous Mater.* **2012**, *153*, 94–99.

[25] M.-J. Díaz-Cabañas, P. A. Barrett, *Chem. Commun.* **1998**, *17*, 1881–1882.

[26] C. W. Andersen, M. Bremholm, P. N. R. Vennestrøm, A. B. Blichfeld, L. F. Lundegaard, B. B. Iversen, *IUCrJ* **2014**, *1*, 382–386.

[27] A. Godiksen, P. N. R. Vennestrøm, S. B. Rasmussen, S. Mossin, *Top. Catal.* **2017**, *60*, 13–29.

[28] C. Tyrsted, E. Borfecchia, G. Berlier, K. A. Lomachenko, C. Lamberti, S. Bordiga, P. N. R. Vennestrøm, T. V. W. Janssens, H. Falsig, P. Beato, A. Puig-Molina, *Catal. Sci. Technol.* **2016**, *6*, 8314–8324.

[29] F. Giordanino, E. Borfecchia, K. A. Lomachenko, A. Lazzarini, G. Agostini, E. Gallo, A. V. Soldatov, P. Beato, S. Bordiga, C. Lamberti, *J. Phys. Chem. Lett.* **2014**, *5*, 1552–1559.

[30] R. Martínez-Franco, M. Moliner, J. R. Thøgersen, A. Corma, *ChemCatChem* **2013**, *5*, 3316–3323.

[31] E. Fernández, M. Moreno-González, M. Moliner, T. Blasco, M. Boronat, A. Corma, *Top. Catal.* **2018**, *61*, 810–832.

[32] F. Gao, Y. Wang, N. M. Washton, M. Kollar, J. Szanyi, C. H. F. Peden, *ACS Catal.* **2015**, *5*, 6780–6791.

[33] Y. Cui, Y. Wang, E. D. Walter, J. Szanyi, Y. Wang, F. Gao, *Catal. Today* **2020**, *339*, 233–240.

[34] A. Godiksen, F. N. Stappen, P. N. R. Vennestrøm, F. Giordanino, S. B. Rasmussen, L. F. Lundegaard, S. Mossin, *J. Phys. Chem. C* **2014**, *118*, 23126–23138, DOI 10.1021/jp5065616.

[35] D. Nielsen, Q. Gao, T. V. W. Janssens, P. N. R. Vennestrøm, S. Mossin, *J. Phys. Chem. C* **2023**, *127*, 12995–13004.

[36] P. C. Bruzzese, E. Salvadori, B. Civalleri, S. Jäger, M. Hartmann, A. Pöppl, M. Chiesa, *J. Am. Chem. Soc.* **2022**, *144*, 13079–13083.

[37] Y. Zhang, Y. Wu, Y. Peng, J. Li, E. D. Walter, Y. Chen, N. M. Washton, J. Szanyi, Y. Wang, F. Gao, *J. Phys. Chem. C* **2020**, *124*, 28061–28073.

[38] M. Moreno-González, B. Hueso, M. Boronat, T. Blasco, A. Corma, *J. Phys. Chem. Lett.* **2015**, *6*, 1011–1017.

[39] J. Song, Y. Wang, E. D. Walter, N. M. Washton, D. Mei, L. Kovarik, M. H. Engelhard, S. Prodinger, Y. Wang, C. H. F. Peden, F. Gao, *ACS Catal.* **2017**, *7*, 8214–8227.

[40] P. C. Bruzzese, E. Salvadori, S. Jäger, M. Hartmann, B. Civalleri, A. Pöppl, M. Chiesa, *Nat. Commun.* **2021**, *12*, 4638.

[41] H. Li, C. Paolucci, I. Khurana, L. N. Wilcox, F. Göltl, J. D. Albarracin-Caballero, A. J. Shih, F. H. Ribeiro, R. Gounder, W. F. Schneider, *Chem. Sci.* **2019**, *10*, 2373–2384.

[42] A. Godiksen, O. L. Isaksen, S. B. Rasmussen, P. N. R. Vennestrøm, S. Mossin, *ChemCatChem* **2018**, *10*, 366–370.

[43] S. A. Bates, A. A. Verma, C. Paolucci, A. A. Parekh, T. Anggara, A. Yezerets, W. F. Schneider, J. T. Miller, W. N. Delgass, F. H. Ribeiro, *J. Catal.* **2014**, *312*, 87–97.

[44] A. Bukowski, L. Schill, D. Nielsen, S. Mossin, A. Riisager, J. Albert, *React. Chem. Eng.* **2020**, *5*, 935–948.

[45] A. L. Godiksen, M. H. Funk, S. B. Rasmussen, S. Mossin, *ChemCatChem* **2020**, *12*, 4893–4903.

[46] S. Shwan, M. Skoglundh, L. F. Lundegaard, R. R. Tiruvalam, T. V. W. Janssens, A. Carlsson, P. N. R. Vennestrøm, *ACS Catal.* **2014**, *5*, 16–19.

[47] B. Gil, B. Marszałek, A. Micek-Ilnicka, Z. Olejniczak, *Top. Catal.* **2010**, *53*, 1340–1348.

[48] M. Ravi, V. L. Sushkevich, J. A. van Bokhoven, *Nat. Mater.* **2020**, *19*, 1047–1056.

[49] S. Stoll, A. Schweiger, *J. Magn. Reson.* **2006**, *178*, 42–55.